Polyhedron 52 (2013) 398–405

Contents lists available at SciVerse ScienceDirect

Polyhedron

journal homepage: www.elsevier.com/locate/poly

Novel paramagnetic-luminescent building blocks containing manganese(II) and anthracene-based curcuminoids

Melita Menelaou [a], Thomas Weyhermüller [b], Mònica Soler [c,*], Núria Aliaga-Alcalde [d,*]

[a] Departament de Química Inorgànica, Universitat de Barcelona, Diagonal 645, 08028 Barcelona, Spain
[b] Max-Planck-Institut für Chemische Energiekonversion Stiftstr. 34-36, 45470 Mülheim an der Ruhr, Germany
[c] Departamento de Ciencia de los Materiales, Facultad de Ciencias Físicas y Matemáticas, Universidad de Chile, Santiago, Chile
[d] ICREA at the Universitat de Barcelona, Diagonal 645, 08028 Barcelona, Spain

ARTICLE INFO

Article history:
Available online 1 September 2012

Dedicated to Alfred Werner on the 100th Anniversary of his Nobel Prize in Chemistry in 1913.

Keywords:
Metal-curcuminoid
Building block
Fluorescence
Magnetism

ABSTRACT

In an effort to study innovative multifunctional molecular materials, two new coordination compounds have been designed containing Mn^{II} as a metallic source and a specific curcuminoid called 9Accm as a chelating ligand. Synthetic reactions were carried out between $Mn(O_2CMe)_2{\cdot}4H_2O$ and 1,7-di-9-anthracene-1,6-heptadiene-3,5-dione (9Accm), leading to $[Mn(9Accm)_2(py)_2]$ (**1**) and $[Mn(9Accm)_2(4,4'\text{-bpy})]_n$ (**2**), respectively. In particular, compound **1** was characterized by analytical, spectroscopic techniques (UV–Vis, fluorescence in the solid state and in solution and EPR), magnetic susceptibility measurements and X-ray crystallography. Compound **2** was characterized by a number of techniques as elemental analysis, UV–Vis, fluorescence (in the solid state and in solution), SQUID magnetic susceptibility studies and EPR. The structure of **1** reveals mononuclear octahedral Mn^{II} species incorporating 9Accm and pyridine while analyses of **2** implies the formation of 1D chain in which Mn^{II} centers bound to 9Accm and link with each other by 4,4-bipyridine molecules. Compound **1** is a mononuclear compound that can act as a potential building block for the design of novel Mn^{II}-curcuminoid species (e.g. compound **2**). Both systems exhibit magnetic properties due to the nature of the metallic source and display fluorescence in the visible region in the solid state and in solution due to the nature of the ligand 9Accm. Therefore, **1** and **2** are excellent examples of multifunctional systems at the molecular scale. Even though both systems are very similar this work depicts the magnetic/fluorescent differences between each other.

1. Introduction

The design of molecular materials with tailored structures and properties is one of the primary goals in nanoscience and nanotechnology [1]. Hence, great efforts are led at the moment toward the formulation of new strategies to create compounds with appealing features at the nanoscale. Such systems will be designed to have electrical, magnetic and optical among others, integrating some of them, the combination of these treats. Related to the latest, in recent years, inspiring materials have been published, showing applications ranging from sensing, catalysis, optoelectronics, etc. [2]. At this point interesting species have been achieved, although most of them by serendipitous methods, lacking on the control of the design and therefore of the final features. At the same time, specialized devices are built for the fabrication of practical systems at the nano-scale, providing further inside on unique molecules and therefore allowing development of useful multifunctional systems.

Related to applications, organic π conjugated molecular systems display appealing properties and are good candidates for optoelectronic nanodevices along with other purposes [3]. Concerning this matter, curcumin (CCM) and its derivates, known as curcuminoids (CCMoids), are promising molecules rather unexplored in the lines of research named above. In general, CCM and CCMoids are described as diarylheptanoid chains that contain β-diketone moieties and aromatic groups on the sides of the chains (Fig. 1). This family of molecules are well-known in biomedicine and exhibit many therapeutic properties being applied as antioxidant, anticancer preventive and anti-inflamatory agents [4,5]. Nowadays, great efforts are devoted to the synthesis of new CCMoids with enhanced biological properties existing, for that matter, several publications in bio-oriented journals [6,4,7,8]. Therefore, there is a library of conjugated systems ready to be investigated. From a designing point of view, CCMoids are versatile molecules: aromatic groups can be tuned, the π conjugation skeleton can also be functionalized and the β-diketone group allows coordination to metal centers. In the case of metal-CCM/CCMoids systems, some

* Corresponding authors.
E-mail addresses: msoler@ing.uchile.cl (M. Soler), nuria.aliaga@icrea.cat (N. Aliaga-Alcalde).

0277-5387/$ - see front matter © 2012 Elsevier Ltd. All rights reserved.
http://dx.doi.org/10.1016/j.poly.2012.08.061

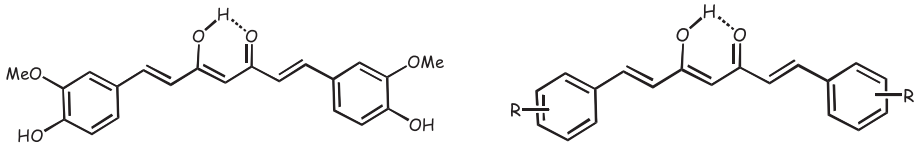

Fig. 1. Representation of curcumin (CCM, left) and general scheme of a curcuminoid. (CCMoid, right). *R* = various.

complexes have been published during the last decades, [9] with few examples containing complete crystallographic data, with only one example with Ru^{III} [10] previous to Cu^{II}, Zn^{II}, Dy^{III} and Yb^{III} compounds published recently by our group [11,12].

In this respect since 2010, a family of compounds containing the CCMoid 9Accm (1,7-(di-9-anthracene-1,6-heptadiene-3,5-dione)) has been achieved and published by us [11]. 9Accm by itself, is a symmetric CCMoid containing anthracene groups that shows interesting fluorescent properties in the visible together with solvatochromic effects [11]. At the nanoscale, the conjugated skeleton of the molecule behaves as a nanowire allowing electronic transport at room temperature between nanoelectrodes (graphite surfaces) [13]. On the other hand, once it coordinates, the nature of the metal provides the possibility of new treats. In this regard, Cu^{II}-9Accm compounds have been studied for bioinorganic purposes and therefore the potential *in vitro* activity was tested [11]. Moreover, Zn^{II}- and Cd^{II}-9Accm species, respectively, have being attained as fluorescent enhancers (while Cu^{II}-9Accm acts as a quencher) and deposition of the Zn^{II}-9Accm species was also carried out [11]. New lanthanides-9Accm species using Dy^{III} and Yb^{III} salts, respectively, have been isolated too, being the first ones of the aforementioned family; a luminescent single-ion magnet and a paramagnetic system which emits in the visible and near-IR regions, respectively [12]. Therefore, the natures of both, ligand and metal, are fundamental in the formation of multifunctional systems and search of applications. Herein, we present the latest studies targeting the Mn^{II}/9Accm system and merging magnetic and luminescent properties together.

2. Experimental

Starting materials were purchased from Aldrich and all manipulations were performed using materials as received. Ligand 9Accm was synthesized as reported elsewhere [11].

2.1. Preparation of $[Mn(9Accm)_2(py)_2]$ (**1**)

2.1.1. Method A

The ligand, 9Accm, (40 mg, 0.084 mmol) was dissolved in DMF (20 ml) and deprotonated with an aqueous solution (5 mL) of LiOH (4 mg, 0.16 mmol). The resulting orange solution was kept under stirring and then, a solution of $Mn(O_2CMe)_2{\cdot}4(H_2O)$ (10.3 mg, 0.042 mmol) in DMF (5 ml) was added dropwise. The final solution was warmed up to 90 °C for three hours and the color of the solution change to dark red. The solution was left under stirring overnight at room temperature. An orange precipitate was formed by concentrating the sample using rotary evaporation. The dry solid was washed with water, methanol and ether and dried in the air. Crystals of **1** were achieved by dissolving the solid in pyridine and layering the solution with ether. Yield: 20%. 1635w, 1550 m, 1505 m, 1440s, 1351w, 1166w, 966w, 781w, 735 m, 699w, 440w. *Anal.* Calc. for **1**·py.H_2O ($C_{80}H_{56}O_4N_2Mn$): C, 80.94; H, 5.03; N, 3.33. Found: C, 80.91; H, 5.09; N, 3.31%. MALDI-TOF ($CHCl_3$/MeCN): m/z: 1006.3 $[Mn(9Accm)_2+H]^+$, 1028.3 $[Mn(9Accm)_2 + Na]^+$, 1192.5 $[Mn(9Accm)_2 + Na + 4MeCN]^+$.

2.1.2. Method B

200 mg of 9Accm (0.42 mmol) were added to 5 mL of pyridine in a microwave tube along with 51 mg (0.21 mmol) of $Mn(O_2CMe)_2{\cdot}4(H_2O)$. The reaction mixture was under continuous stirring while applying a power of 250 microwave energy for 2 min. The temperature was allowed to reach 140 °C and then left to drop to room temperature. Finally, a yellow microcrystalline material was obtained. The compound was washed with water, MeOH and ether. Yield: 67%. The IR of the compound was identical to the crystals achieved by Method A after layering.

2.2. Synthesis of $[Mn(9Accm)_2(4,4'\text{-bpy})]_n$ (**2**)

100 mg of 9Accm (0.21 mmol) were added to 5 mL of DMF in a microwave tube together with 25 mg (0.11 mmol) of $Mn(O_2CMe)_2{\cdot}4(H_2O)$ and 17 mg (0.11 mmol) of 4,4′-bpy. The microwave reaction was performed following the same methodology described above. A dark red solution was obtained and left undisturbed overnight. This way, a dark orange precipitate was attained; the solid was filtered and washed with water, MeOH, and Ether. Yield: 63%. IR (ν/cm^{-1}) 1663 m, 1627w, 1549w, 1505 m, 1440 m, 1157w, 983w, 881w, 734w, 604w, 541w, 448w. *Anal.* Calc. for **2**·$4.5H_2O{\cdot}0.25$DMF ($C_{90}H_{62}O_4N_4Mn$): C, 76.76; H, 5.32; N, 2.49. Found: C, 76.78; H, 5.11; N, 2.18%. MALDI-TOF ($CHCl_3$/MeCN): m/z: 1006.3 $[M(9Accm)_2 + H]^+$, 1028.3 $[Mn(9Accm)_2 + Na]^+$, 1161.3 $(Mn(9Accm)_2(4,4'\text{-bpy})-1e^-)$, 1192.5 $[Mn(9Accm)_2 + Na + 4MeCN]^+$.

2.3. Physical measurements

C, H and N analyses were performed with a Perkin-Elmer 2400 series II analyzer. MALDI-TOF spectra of **1** and **2** were recorded in $CHCl_3$/MeCN in a 4800 plus MALDI TOF/TOF (ABSciex-2010) spectrometer. Infrared spectra (4000–400 cm^{-1}) were recorded from KBr pellets on a Bruker IFS-125 FT-IR spectrophotometer. Absorption spectra were recorded with 1 nm resolution for all cases on a Cary 100 Bio UV-spectrophotometer. Microwave experiments were performed with the CEM Focused Microwave Synthesis System, Model Discover.

2.4. Structure determination

Data for compound **1** were collected on a pinkish red plate on a Bruker Kappa-Mach3/APEXII-CCD diffractometer equipped with a Mo-target rotating anode setup and an Incoatec-Helios-Mirror monochromator. Final cell constants were obtained from a least squares fit of several thousand strong reflections. The structure was readily solved with the Patterson method and subsequent difference Fourier techniques. Refinement on F^2 was performed with the SHELXTL suite [14]. All non-hydrogen atoms were refined anisotropically. Hydrogen atoms were placed at calculated positions and isotropically refined as riding atoms.

2.5. Fluorescence data

Fluorescence emission spectra in the solid state and in solution were carried out on a Horiba-Jobin–Yvon SPEX Nanolog-TM and a

Cary Eclipse spectrofluorimeter. Only distilled solvents were employed and concentrations of 9Accm and compounds **1** and **2** were 10^{-5} M for all three systems. The slits used were of 3 nm for all the experiments.

2.6. Magnetic experiments

X-band EPR data of **1** were collected in solution (DMF and toluene) with a Bruker ELEXSYS E500 spectrometer at the Max-Planck Institute für Bioanorganische chemie. Solid EPR data of **1** and **2** were collected with a Bruker ESP300E at the Scientific Services of the University of Barcelona. Magnetic experiments using SQUID were performed in the "Unitat de Mesures Magnètiques (Universitat de Barcelona)" on polycrystalline samples with a Quantum Design SQUID MPMS-XL magnetometer working in the 2.0–300 K range. The magnetic fields were 0.02 T (from 2 to 30 K) and 0.3 T (from 30 to 300 K) for **1** and 0.3 T from 2 to 300 K for **2**, respectively. The diamagnetic corrections were evaluated from Pascal's constants.

2.7. Crystal Structure [Mn(9Accm)$_2$(py)$_2$] (**1**)

A labeled ORTEP representation is depicted in Fig. 2 (left). Crystallographic data of compound **1** are collected in Table S1.

Compound **1** crystallizes in the monoclinic space group P2(1)/c with the asymmetric unit containing two molecules of **1**. Compound **1** contains a hexacoordinated Mn^{II} ion with an octahedral geometry lying on an inversion center. The central manganese ion is coordinated to two 9Accm ligands by 4 oxygen atoms from the β-diketone group forming an equatorial plane, while in the apical positions the manganese ion is coordinated to two pyridine molecules by the two N atoms. The bond distances around the manganese ion are Mn(1)-O(17) and Mn(1)-O(19) with bond lengths of 2.1380 Å and 2.1614 Å, respectively, and Mn(1)-N(41) with bond lengths of 2.3311 Å, all in accordance with similar bond distances reported in the literature for a Mn^{II} ion coordinated to the oxygen atoms of β-diketone groups and Mn^{II} ion coordinated to pyridine ligands. The bond angles around the Mn^{II} ion are also in good agreement with previously observed, being the bond angle O(19)-Mn(1)-O(17) of 85.09°, forming a 6-membered ring between the Mn^{II} ion and the β-diketone, while the bond angle O(19)-Mn(1)-O(17') outside the 6-membered ring is 94.91° [15]. Diagonal angles around the octahedron formed around the Mn^{II} all are shown to be 180° (O(17)-Mn(1)-O(17'), O(19)-Mn(1)-O(19) and N(41)-Mn(1)-N(41)). Bond distances within the 9Accm ligand show average single (C-C) and double (C-C) bond distances depicted in related conjugated diarylheptanoid systems [11,12]. Bond distances and angles are listed in Tables S2 and S3.

Looking at the geometrical arrangement of the ligands surrounding the central Mn^{II} ion (Fig. 3), the anthracene groups for the 9Accm ligands are oriented perpendicular to the skeleton of the conjugated ligand and to the equatorial plane of the molecule, the same as the two pyridine molecules. It can also be seen that the two anthracene groups are again tilted from the conjugated skeleton (Figs. 2 and 3) as previously reported for the [Zn(9Accm)$_2$(py)] analog [11].

The structure of compound **1** is the fourth example of a crystal structure of a 9Accm curcuminoid ligand coordinated to a transition metal ion reported in the literature, following the structures of the divalent metal ions Zn^{II} and Cu^{II}, namely [Zn(9Accm)$_2$(py)] and [Cu(9Accm)$_2$(py)] and [(Phen)CuCl(9Accm)] [11]. Another example of curcumin coordinated to a metal is the case of Ru which was previously reported [10]. Interestingly, comparing the structure of compound **1** with the aforementioned structures, in all cases the structures show the flexibility of the 9Accm ligand. Moreover, in the case of the two species [Zn(9Accm)$_2$(py)] and [Cu(9Accm)$_2$(py)], no intermolecular interactions were observed, while in an analogous species, namely [(phen)CuCl(9Accm)] weak π-stacking interactions among the phenanthroline units and the phenanthroline-anthracene groups were described. In compound **1**, Van der Waals interactions between two pyridine ligands of different molecules (Fig. 2 right) can be observed with distances N(41)-C(43′)/ N(41′)-C(43) of 3.417 Å, C(42)-C(43′)/C(42′)-C(43) of 3.328 Å, and C(42)-C(44′)/C(42′)-C(44) of 3.398 Å. respectively [11].

Therefore, herein the first example of a family of species which arose from the system of Mn^{II} and a curcuminoid ligand (9Accm) is presented, gaining information first on the high affinity of the aforementioned well defined ligand towards the divalent metal ion Mn(II) and second gaining more information on the promising

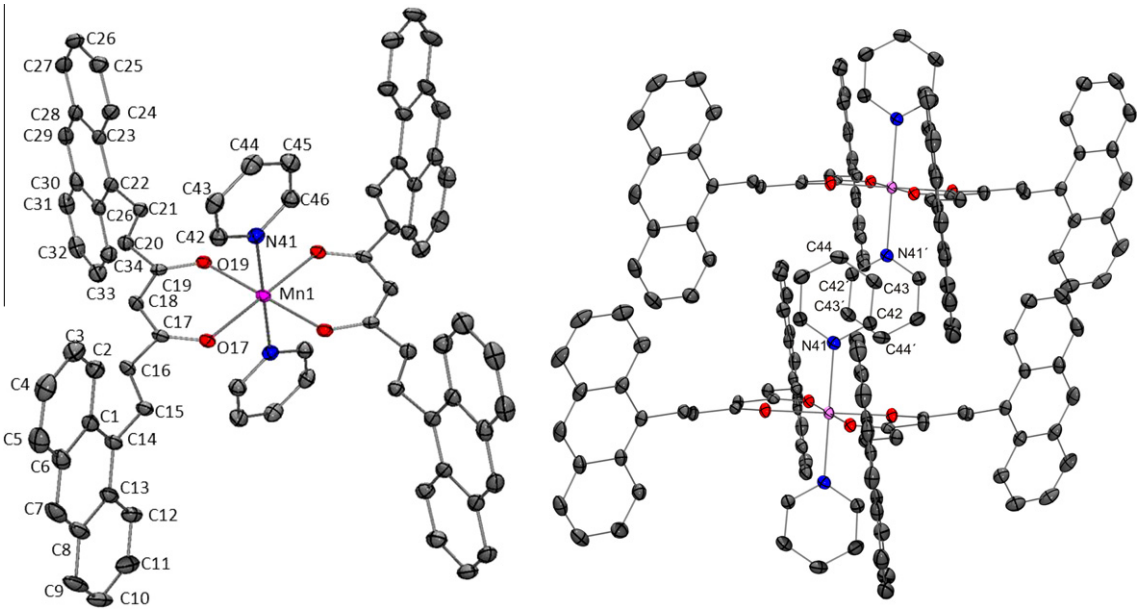

Fig. 2. (Left) POV-Ray labeled ORTEP representation of [Mn(9Accm)$_2$(py)$_2$]. (Right) Figure showing the atoms involved in the Van der Waals interactions between two pyridine groups of different molecules.

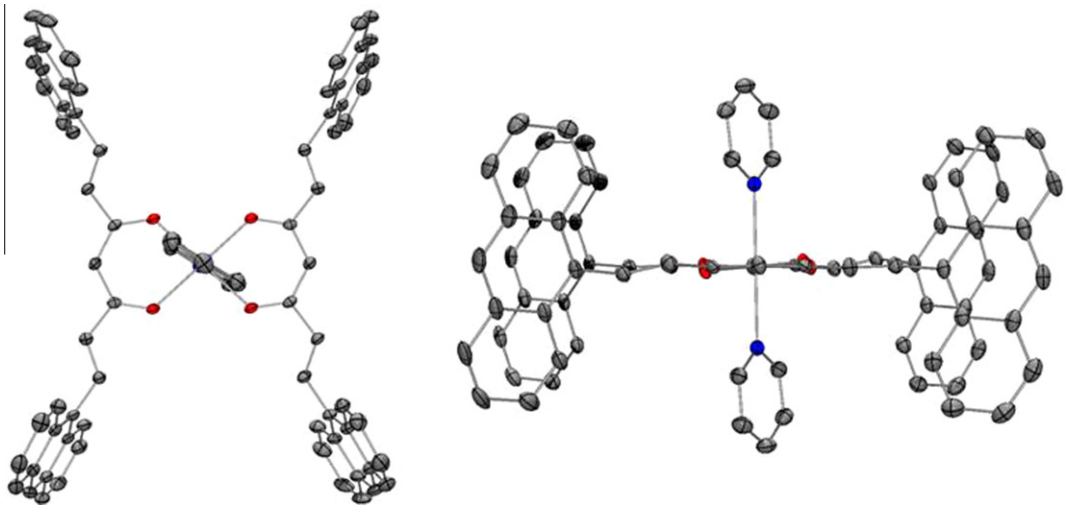

Fig. 3. (Left) View of the equatorial plane. (Right) Perpendicular view of the equatorial plane.

family of curcuminoid metal coordinated compounds in the presence of 3d and/or 4f metal ions.

3. Discussion

The present work describes the formation of a mononuclear complex, $[Mn(9Accm)_2(py)_2]$ (**1**), when $Mn(O_2CMe)_2$ and 9Accm are added in a ratio 1:2, respectively, and a 1D system $[Mn(9Accm)_2(4,4'\text{-bpy})]_n$ (**2**), by introducing a linker (1:2:1, Mn:9Accm:4,4′-bipyridine, Fig. 4). Even though both results were expected (because of the nature of the starting materials involved) it is still notable the self-assembly process that takes place by adding all the reagents together in the correct ratio. Two synthetic methodologies were followed in the achievement of **1**; the first implied the use of base to deprotonate the ligand together with the application of temperature, improving the solubility of the ligand and therefore its reactivity in solution in the presence of the metal ion; the second synthetic path was related to the use of a microwave reactor. The latest methodology shows remarkable improvements compared with the initial one; microwave reactions allow the increase of the amount of starting materials decreasing spectacularly the volume of solvent. It is possible to attain pure compounds with excellent yields in a short period of time (20 min average). Therefore, the application of microwave sources on this type of reactions is of great interest, being able of achieving mononuclear systems (e.g. **1**) and/or developed species (e.g. **2**) depending on the ligands involved. Even more, liquid reagents and potential ligands (as it happens with pyridine in compound **1**) can be used as unique solvents in this type of reactions and single crystals can grow directly from the reactions taken into account temperature and solubility factors, respectively.

The crystal structure of **1** shows the exact coordination mode of the mononuclear building block and provides an idea of potential designs by exchanging pyridine molecules (for example 1D systems (**2**), Fig. 4 right). In fact compound **1** is sequentially repeated in **2** where, 4,4′-bpy was initially used to avoid possible steric problems between building blocks ($Mn(9Accm)_2$ entities). Despite the absence of crystallographic data for **2**, spectroscopic analyses performed on the material clearly demonstrates the formation of a 1D-chain along with additional factors, such as a remarkable decrease of the solubility of this material compared to **1**. The comparison of the FT-IR spectra of these complexes provides valuable information (Fig. S1). Indeed, the broad band observed between 2800 to 3200 cm^{-1} for the free 9Accm is, as expected, missing in both compounds due to the lost of a proton and coordination of the β-diketone moiety to a metal center [16]. In general, both complexes, **1** and **2**, show a medium-sized band at ~1626–1635 cm^{-1} followed by three other single bands around 1550, 1504 and 1440 cm^{-1} which intensities grow almost progressively. All of them are assignable to the $\nu_{(C=O)}$, $\nu_{(C=N)}$ and $\nu_{(C=C)}$ stretching moieties. A characteristic $\nu_{(C-H)}$ band from anthracene group appears also in both at 734 cm^{-1}. Below 650 cm^{-1} only weak vibrations were observed, none of them assignable to $\nu_{(M-O)}$. However, two significant changes appear once the two compounds are compared:

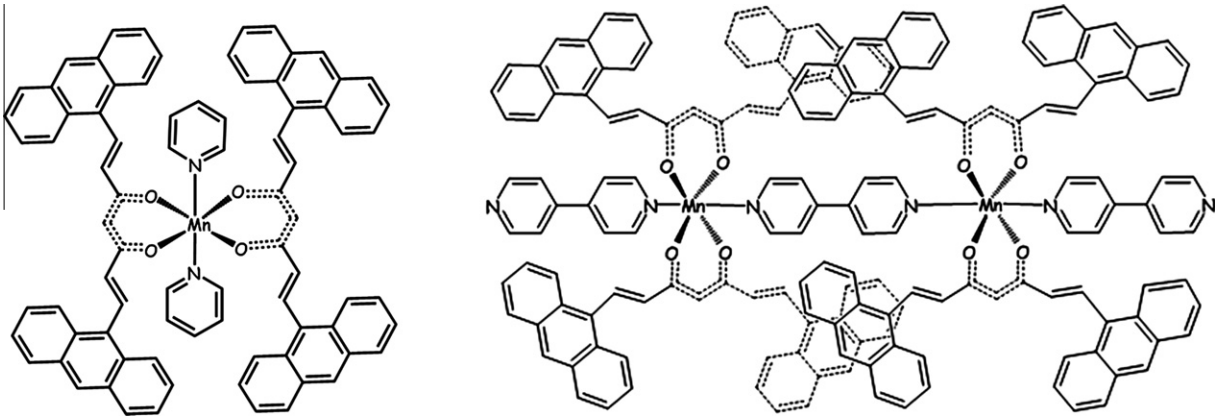

Fig. 4. Artist's impression of compounds **1** (left) and **2** (right), respectively.

(i) two bands at 1675 and 1663 cm^{-1} appears for **2** being missing in **1** probably relating to the vibrational modes of DMF (used in the synthesis of **2**) and/or molecules of water [17]. (ii) Complex **1** exhibits two peaks at 780 and 697 cm^{-1} due to coordinated and free pyridine molecules. The latest are missing in **2**. MALDI mass spectra confirmed the existence of $[Mn(9Accm)_2 + H^+]$, $[Mn(9Accm)_2 + Na^+]$ and $[M(9Accm)_2 + Na + 4MeCN]^+$ species for the two compounds but in the case of **2** additional $(Mn(9Accm)_2(4,4'\text{-bpy})–1e^-)$ moieties were also detected. The elemental analyses fit very well with the nitrogen percentage expected in both cases, showing the existence of a 4,4′-bipyridine molecule per $[Mn(9Accm)_2]$ unit (Fig. 4 right). Regarding this system, present work involves small axial ligands (e.g. pyrazine) that may add/improve features in the final 1D species as for example strength of the magnetic exchange between Mn^{II} ions within the chain compared with 4,4′-bpy (see below).

3.1. EPR and SQUID measurements

The magnetic characterization of **1** and **2** were performed by means of magnetic susceptibility data (microcrystalline solid, Figs. 5 and S2, respectively) and X-band EPR (solid state, powder, for both and solution (DMF and toluene) in the case of **1**; see Fig. 6).

The data for compound **1** show a behavior characteristic of mononuclear Mn^{II} species. The $\chi_M T$ value decreases from 4.68 $cm^3\ mol^{-1}$ K at 300 K to 4.06 $cm^3\ mol^{-1}$ K at 2 K, very similar to that expected for a magnetically isolated $S = 5/2$ system ($\chi_M T = 4.375\ cm^3 mol^{-1} K$ assuming $g = 2.0$). A regular plateau is observed until very low temperatures and then a fast drop of the magnetic susceptibility is observed (Fig. S2). Correlation of the magnetic data above 100 K were performed using the Curie–Weiss law where the best fitting provided values of $C = 4.69\ cm^3 mol^{-1} K$ and $\theta = -3.11$ K (Fig. 5) [18]. The aforementioned fitting results match well with this supramolecular pattern and correlations were improved when intermolecular interactions were taken into account. The value of θ is in the order of others reported in the literature and its antiferromagnetic nature agrees with the falling of the magnetic susceptibility at the lowest temperatures. Magnetization measurements were carried out at 2 K and in the field range 0–5 T. The results are shown in Fig. 5 along with the theoretical Brillouin function of an $S = 5/2$ system. The non-coincidence of the two curves is probably due to slight variations on the g value ($g = 2.0$ for the simulation) and small intermolecular interactions that take relevance at very low temperatures. The above is consistent with the crystallographic information of **1** that shows the existence of intermolecular π–π interactions among the mononuclear units through the pyridine molecules, (Fig. 2 right, few C···C/N distances around 3.4 Å) forming a supramolecular entity with a preferred direction (similar to the 1D chain of **2**, see Fig. 4). On the other hand, the disposition of the aromatic rings from the anthracene groups protects the supramolecular chains from each others.

The χ_M and $\chi_M T$ versus T plots for **2** are shown in Fig. S2. It was observed that the magnetic susceptibility data decreased smoothly upon cooling, from 4.65 $cm^3\ mol^{-1} K$ at 300 K to a value of 3.58 $cm^3\ mol^{-1} K$ at 3 K, which suggests weak antiferromagnetic interactions. The experimental data was analyzed by Fisher's expression for an uniform chain based on the Hamiltonian $H = -J\Sigma S_i S_{i+1}$, with $S = 5/2$ [19]. A good fitting was obtained above 10 K with $g = 2.0$ (fixed), $J = -0.2\ cm^{-1}$ and TIP = $200 \times 10^{-5}\ cm^3 mol^{-1}$. The resulting values fit well with the shape of the graph as well as with previous bibliography; It is known that the exchange coupling through 4,4′-bipyridine molecules is very weak providing low values, comparable sometimes with intermolecular interactions [20].

In addition, X-band EPR experiments were performed for both **1** and **2**. Compound **1** was studied in solution (DMF and toluene) and in the solid state at 4 K; **2** was compared to **1** in the solid state under the same conditions. The experiments depict the anticipated features in the case of the mononuclear Mn^{II} system (**1**) and changes related to the formation of a 1D system (**2**). The spectra in DMF and toluene of **1** depict many features observed in mononuclear high spin Mn^{II} species. This way, a sharp resonance around $g = 2$ exhibiting six-line hyperfine splitting. Also, a broad weak signal around $g = 5$ is observed. Overall, these are indications that **1** retains its structure in solution. However, in the solid state at 4 K, compounds **1** and **2** depict distinctive spectra. None of the spectra present hyperfine transitions now making more complicated a detailed interpretation of the data. Both compounds present an intense resonance around $g = 2.0$ with weak resonance on both the low- and high-fields sides of the main resonance (Fig. 6). Compound **2** depicts them in a more symmetric pattern than **1**, being both species clearly different. In the absence of further theoretical studies, these results suggest small zero-field splitting parameters, lower in value than the X-band microwave frequency. Normally $|D|$ values for mononuclear Mn^{II} are between 0 and 0.20 cm^{-1} [21]. The line widths observed in the solid state for both systems may relate to phenomena as unresolved ligand hyperfine interactions, distributions of D and E values, spin-lattice and spin–spin relaxation [22]. In the case of **2**, the small but present exchange interactions between the Mn^{II} centers may also be an additional factor to be taken under account.

3.2. Uv–Vis & luminescence

The UV–Vis spectroscopy of compounds **1** and **2** were conducted in CH_2Cl_2 (final concentrations 10^{-5} M) and compared with

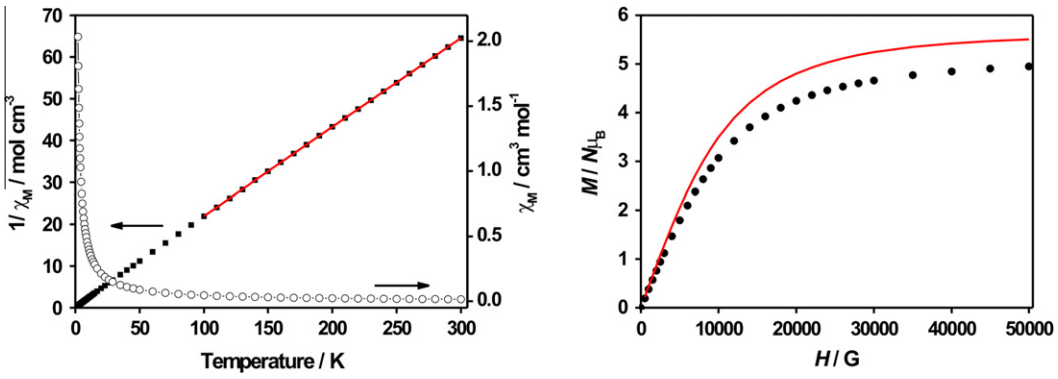

Fig. 5. (Left) $1/\chi_M$ vs. T (black dots) and χ_M vs. T (white dots) spectra. The fitting result is depicted by a red line. (Right) M vs. H representation, the experimental data is depicted using black spheres and the simulation using Brillouin function with a red line. (Color online.)

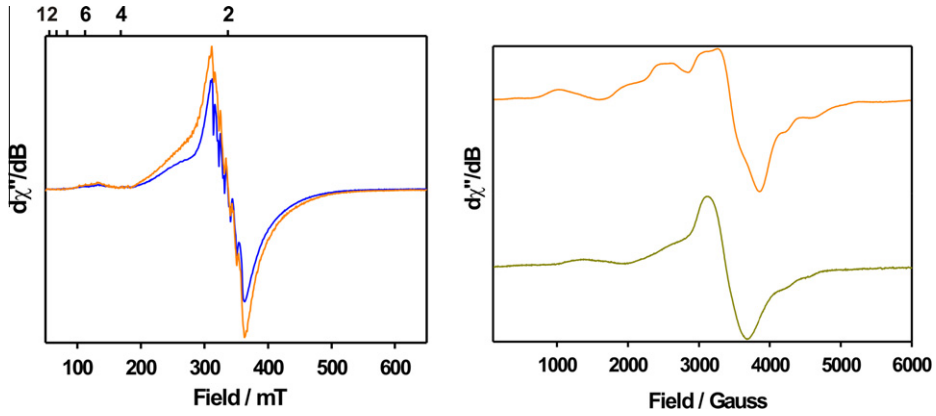

Fig. 6. (Left) X-band EPR spectra of compound **1** in DMF (orange) and toluene (blue). (Right) X-band solid EPR of compound **1** (top, orange) and **2** (bottom, olivetone). (Color online.)

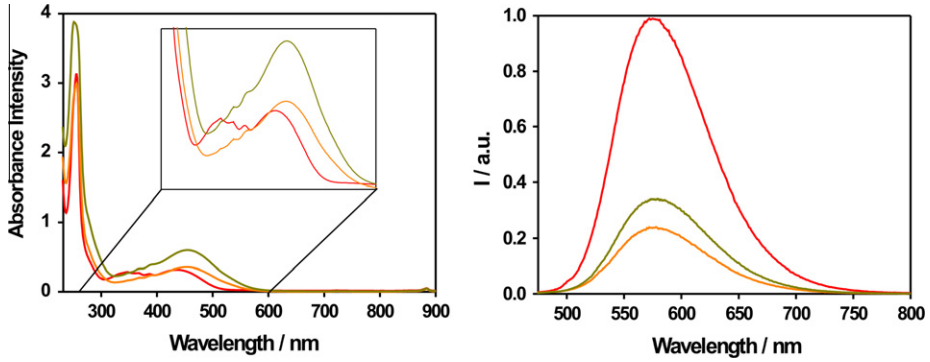

Fig. 7. (Left) UV–vis spectra of 9Accm (red), **1** (orange) and **2** (olivetone) of solutions 10^{-5} M in CH_2Cl_2. The inset shows the features of all three species between 240 and 600 nm. (Right) Fluorescence spectra of the three systems following the same color legend of solutions 10^{-5} M in CH_2Cl_2. (Color online.)

the free ligand under the same conditions. The electronic spectra of all three are shown in Fig. 7. Overall, the two compounds display similar features comparable also to other metal curcuminoid systems [11,12]; at 256 and 251 nm (ε = 299 (**1**) and 388 (**2**) M^{-1}-cm^{-1}), in that order, sharp and intense bands are observed assigned to $\pi \rightarrow \pi$ transitions [11]. Between 300 and 600 nm, compounds **1** and **2** show a broad band at 453 and 455 nm, respectively, red shifted from the free ligand (Fig. 7), and well-resolved vibrational bands related to the anthracene groups between 300 and 400 nm. Such features have been already observed and analyzed in similar Zn^{II} and Cu^{II} compounds containing 9Accm [11].

Emission spectra were recorded in the solid state as well as in CH_2Cl_2 (10^{-5} M) upon excitation at 365, 390 and 455 nm. In solution, compounds **1** and **2** show single broad bands with both maxima at 576 nm (Fig. 7). This is very similar to the free ligand, 9Accm, which maximum at such conditions is at 575 nm. No emission was observed when samples are excited below 300 nm. The Mn^{II} systems (**1** and **2**) show partial quenching phenomena comparing with free 9Accm; it should be taken also into account that this qualitative comparison was performed at the same concentrations (in **1** and **2** each metal center coordinated to two ligands) and still show lower fluorescence intensity. These facts are related to

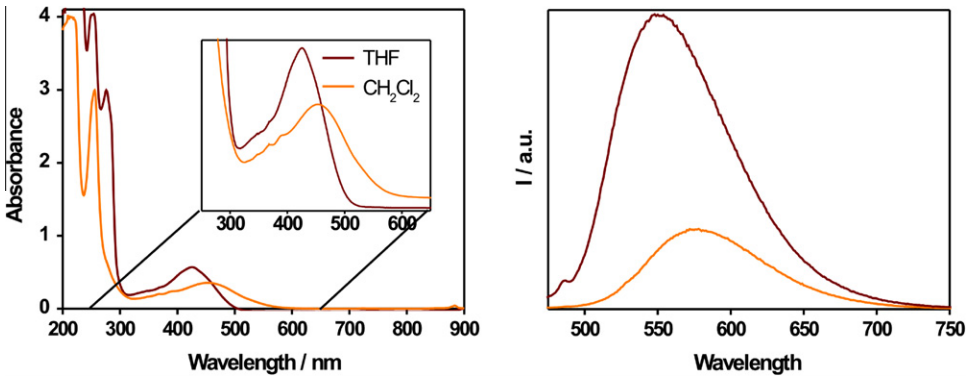

Fig. 8. (Left) UV–vis spectra of **1** 10^{-5} M in CH_2Cl_2 (orange) and **1** 10^{-5} M in THF (maroon) of solutions. The inset shows the features of all species between 250 and 650 nm. (Right) Fluorescence spectra of **1** 10^{-5} M in CH_2Cl_2 (orange) and **1** 10^{-5} M in THF (maroon) of solutions. Intensities are referred to the most intense band (maroon color). (Color online.)

the coordination of 9Accm to paramagnetic centers [23]. In addition, it is observed that, in solution, compound **2** has higher absorption and emission bands than **1**; fact that could be related to the coordination of the former to the 4,4'-bpy ligand that may assist in the processes; further studies should be undertaken to verify the fact as well as to get insight information of the nature of the transitions for both compounds. The effect of solvent was tested with **1** using THF instead of CH_2Cl_2. As a consequence, a shift of the absorption and emission bands of the compound was observed. The changes present in the UV–Vis may be related to the partial or total occupation of the axial positions (pyridine molecules) by THF molecules (also coordinating). Concerning fluorescence the maximum emission was found at 550 nm, shifted 26 nm to the blue region from the one observed in distilled CH_2Cl_2 which is in agreement with the shift in the absorption spectrum (Fig. 8). Previous studies of the free ligand in THF showed that 9Accm appears at 555 nm. In comparison, compound **1** emission appears shifted to the blue as it was the case for Cd^{II} and Zn^{II} compounds using the same solvent [11].

In addition, the emission spectra of **1** and **2** in the solid state show mainly single bands for each compound similar in shape to the ones observed in solution (emission of **1** appears at 656 and **2** at 658 nm, respectively) but shifted to the red region by 80 nm in the case of **1** and 82 nm for **2** (Fig. S3); the shift may directly relate to intermolecular interactions between the molecules as well as the intensities of the emissions for both samples, where this time compound **2** presents a drastic fluorescent quench comparing with **1**. Altogether compounds **1** and **2** combine fluorescent and magnetic properties, being specially promising candidates for luminescent molecular magnetic materials.

4. Conclusions

The present work is the new addition to a new family of 3d coordination compounds containing 9Accm, a curcuminoid group, which here it coordinates to Mn^{II} centers to provide mononuclear as well as 1D species, depending on additional axial ligands (pyridine (py) and 4,4′-bipyridine (4,4'-bpy), in that order). Our general goal is the creation of multifunctional molecular building blocks and the search of advance systems using such units. For that matter, the manuscript introduces two novel compounds named as **1**, $[Mn^{II}(9Accm)_2(py)_2]$ and **2**, $[Mn^{II}(9Accm)_2(4,4'\text{-bpy})]_n$, respectively. Compound **1** has been characterized by standard techniques and X-ray diffraction; compound **2** by the former and by means of comparison with **1**.

Both species present magnetic and fluorescent properties. Compound **1** displays the expected magnetic response of a $S = 5/2$ species, exhibiting magnetic susceptibility data as well as X-band EPR spectra in solution that corroborates this fact. X-band EPR in the solid state was also performed and it did show a very different pattern than in solution, being the line width probably related to the sum of several factors as unresolved hyperfine interactions, distributions of axial and perpendicular zero field splitting parameters, spin lattice, etc. Compound **2** presents smooth changes in the magnetic susceptibility curve, showing a weak antiferromagnetic behavior, characteristic of chains containing 4,4′-bpy units. Also, it shows a cleaner solid X-band EPR spectrum compared with **1**, among other factors due to the weak intermolecular interaction between the Mn^{II} centers through the 4,4′-bipyridine molecules, which also play an important role separating the metallic centers from each other (in **1**, pyridine molecules from one compound intercalate within neighboring molecules). Systems **1** and **2** present fluorescence on the visible (around 575 nm) due to fluorophors that form part of the coordinated ligands. Both species present partial quenching of the fluorescence compared with free 9Accm, fact that it is expected in paramagnetic systems. Solvatochromic effects were tested with **1** by using THF instead of CH_2Cl_2, observing a considerable shift to the blue in the case of the former. In the solid state, both compounds display fluorescent features shifted to the red due to the intermolecular interactions, and interestingly compound **2** presents a much lower fluorescent intensity than in **1**.

This work presents the preliminary data obtained with Mn^{II} and 9Accm for the formation of multifunctional molecules and polymers. Herein, our aim has been to provide an initial evaluation of how properties can vary depending on the nature (molecular or polymeric) of the final compounds. Compounds **1** and **2** are prototypes similar in nature but showing different traits. The evaluation and understanding of such variations is vital to provide improved systems. Further fluorescent studies (lifetime and quantum yield) together with theoretical studies will be performed to fully understand the nature of these variations. Ultimately, both systems should be tested on surfaces to evaluate their final applications on nanodevices.

Acknowledgements

The authors thank the Ministerio de Educación y Ciencia (CTQ2009-06959/BQU), AGAUR fellowship (2008 BE1 00463) and FONDECYT GRANT 1110206 for financial support. N.A.A. also thanks Dr. Núria Clos from the Scientific Technical Services of Diagonal Campus at the University of Barcelona.

Appendix A. Supplementary data

Supplementary data associated with this article can be found, in the online version, at http://dx.doi.org/10.1016/j.poly.2012.08.061.

References

[1] (a) G.M. Whitesides, Small 1 (2005) 172;
(b) A.J. Nozik, Nano Lett. 10 (2010) 2735;
(c) T.W. Odom, M.-P. Pileni, Acc. Chem. Res. 41 (2008) 1565.
[2] (a) D. Maspoch, D. Ruiz-Molina, J. Veciana, Chem. Soc. Rev. 36 (2007) 770;
(b) A.B. Gaspar, V. Ksenofontov, M. Seredyuk, P. Gütlich, Coord. Chem. Rev. 249 (2005) 2661;
(c) E. Chelebaeva, J. Larionova, Y. Guari, R.A.S. Ferreira, L.D. Carlos, F.A.A. Paz, A. Trifonov, C. Guérin, Inorg. Chem. 47 (2008) 775;
(d) S. Decurtins, R. Pellaux, G. Antorrena, F. Palacio, Coord. Chem. Rev. 190–192 (1999) 841;
(e) S. Nemat-Nasser, S. Nemat-Nasser, T. Plaisted, A. Starr, A. V. Amirkhizi, Biomimetics: Biologically Inspired Technologies edited by Yoseph Bar-Cohen, CRC Press (2005).
[3] (a) Y. Shirota, J. Mater. Chem. 10 (2000) 1;
(b) H. Sirringhaus, N. Tessler, R.H. Friend, Science 280 (1998) 1741;
(c) R. Yang, Y. Xu, X.-D. Dang, T.-Q. Nguyen, Y. Cao, G.C. Bazan, J. Am. Chem. Soc. 130 (2008) 3282.
[4] H. Hatcher, R. Planalp, J. Cho, F.M. Torti, S.V. Torti, Cell. Mol. Life Sci. 65 (2008) 1631.
[5] J. Milobedzka, S.V. Kostanecki, V. Lampe, Chem. Ber. 43 (1910) 2163.
[6] H.J.J. Pabon, Rec Tray Chim Pays-Bas Belg 83 (1964) 379.
[7] H. Ohtsu, H. Itokawa, Z. Xiao, C.-Y. Su, C.C.-Y. Shih, T. Chiang, E. Chang, Y. Lee, S.-Y. Chiu, C. Chang, K.-H. Lee, Bioorg. Med. Chem. 11 (2003) 5083.
[8] F. Kuhlwein, K. Polborn, W.Z. Becl, Anorg. Allg. Chem. 623 (1997) 1211.
[9] (a) K. Krishnankutty, P. Venugopalan, Synth. React. Inorg. Met.-Org. Chem. 28 (8) (1998) 1313;
(b) M. Borsari, E. Ferrari, R. Grandi, M. Saladini, Inorg. Chim. Acta 328 (2002) 61;
(c) K. Krishnankutty, V.D. John, Synth. React. Inorg. Met-Org. Nano-Met. Chem. 33 (2003) 343;
(d) V.D. John, K. Krishnankutty, Trans. Met. Chem. 30 (2) (2005) 229;
(e) V.D. John, K. Krishnankutty, Appl. Organomet. Chem. 20 (8) (2006) 477;
(f) K. Krishnankutty, J. John, B. Joseph, J. Ind. Chem. Soc. 84 (2007) 478;
(g) G. Modi, K.S. Pitre, J. Coord. Chem. 62 (2009) 931;
(h) Y.-M. Song, J.-P. Xu, L. Ding, Q. Hou, J.-W. Liu, Z.-L. Zhu, Inorg. Biochem. 103 (2009) 396;
(i) B. Zebib, Z. Mouloungui, V. Noirot, Bioorg. Chem. App. (2010) 1;
(j) X.-Z. Zhao, T. Jiang, L. Wang, H. Yang, S. Zhang, P. Zhou, J. Mol. Struct. 984 (2010) 316;
(k) V.D. John, K. Krishnankutty, Met. Chem. 33 (2010) 157;

(l) M. Sagnou, D. Benaki, C. Triantis, T. Tsotakos, V. Psycharis, C.P. Raptopoulou, I. Pirmettis, M. Papadopoulos, M. Pelecanou, Inorg. Chem. 50 (2011) 1295.
[10] F. Kuhlwein, K. Polborn, W. Beck, Z. Anorg. Allg. Chem. 623 (1997) 1211.
[11] (a) N. Aliaga-Alcalde, P. Marqués-Gallego, M. Kraaijkamp, C. Herranz-Lancho, H. den Dulk, H. Görner, O. Roubeau, S.J. Teat, T. Weyhermüller, J. Reedijk, Inorg. Chem. 49 (2010) 9655;
(b) N. Aliaga-Alcalde, L. Rodríguez, M. Ferbinteanu, P. Höfer, T. Weyhermüller, Inorg. Chem. 51 (2012) 864;
(c) N. Aliaga-Alcalde, L. Rodríguez, Inorg. Chim. Acta 380 (2012) 187.
[12] M. Menelaou, F. Ouharrou, L. Rodríguez, O. Roubeau, S.J. Teat, N. Aliaga-Alcalde, Chem. A Eur. J. (2012). ID: chem.201200955.
[13] F. Prins, A. Barreiro, J.W. Ruitenberg, J.S. Seldenthuis, N. Aliaga-Alcalde, L.M.K. Vandersypen, H.S.J. van der Zant, Nano Lett. 11 (11) (2011) 4607.
[14] G.M. Sheldrick, Acta Crystallogr., Sect. A 64 (2008) 112.
[15] (a) D.F. Xiang, C.Y. Duan, X.S. Tan, Y.J. Liu, W.X. Tang, Polyhedron 17 (1998) 2647;
(b) Y.J. Jang, U. Lee, B.K. Koo, Bull. Korean Chem. Soc. 26 (2005) 925.
[16] G. Aromí, P. Gamez, O. Roubeau, P.C. Berzal, H. Kooijman, A.L. Spek, W.L. Driessen, J. Reedijk, Inorg. Chem. 41 (2002) 3673.
[17] (a) M.X. Li, G.Y. Xie, Y.D. Gu, J. Chen, P.J. Zheng, Polyhedron 14 (1995) 1235;
(b) T. Bataille, F. Costantino, P. Lorenzo-Luis, S. Midollini, A. Orlandini, Inorg. Chim. Acta 361 (2008) 9.
[18] (a) O. Kahn, Molecular Magnetism, VCH, New York, 1993. pp. 11;
(b) M. Matzapetakis, N. Karligiano, A. Bino, M. Dakanali, C.P. Raptopoulou, V. Tangoulis, A. Terzis, J. Giapintzakis, A. Salifoglou, Inorg. Chem. 39 (2000) 4044.
[19] M.E. Fisher, Am. J. Phys. 32 (1964) 343.
[20] (a) X.-L. Hong, J. Bai, Y. Song, Y.-Z. Li, Y. Pan, Eur. J. Inorg. Chem. (2006) 3659;
(b) Y.-S. Ma, X.-Y. Tang, F.-F. Xue, B. Chen, Y.-L. Dai, R.-X. Yan, S. Roy, Eur. J. Inorg. Chem. (2012) 1243.
[21] S. Naskar, D. Mishra, S.K. Chattopadhyay, M. Corbella, A.J. Blake, Dalton Trans. (2005) 2428.
[22] L.R. Gahan, V.A. Grillo, T.W. Hambley, G.R. Hanson, C.J. Hawkins, E.M. Proudfoot, B. Moubaraki, K.S. Murray, D. Wang, Inorg. Chem. 35 (1996) 1039.
[23] E. Tamanini, K. Flavin, M. Motevalli, S. Piperno, L.A. Gheber, M.H. Todd, M. Watkinson, Inorg. Chem. 49 (2010) 3789.